Am J Transl Res 2018;10(8):2335-2349
www.ajtr.org /ISSN:1943-8141/AJTR0075897

Original Article

Direct factor Xa inhibition attenuates acute lung injury progression via modulation of the PAR-2/NF-κB signaling pathway

Meng Shi[1,3*], Linlin Wang[2,3*], Jian Zhou[2,3], Shimeng Ji[2,3], Ningfang Wang[2,3], Lin Tong[2,3], Jing Bi[2,3], Yuanlin Song[2,3], Jie Hu[2,3], Xiaofeng Chen[1]

[1]Department of Cardiothoracic Surgery, Huashan Hospital, Fudan University, Shanghai, China; [2]Department of Pulmonary Medicine, Zhongshan Hospital, Fudan University, Shanghai, China; [3]Shanghai Respiratory Research Institution, Shanghai, China. [*]Co-first authors.

Received March 12, 2018; Accepted June 23, 2018; Epub August 15, 2018; Published August 30, 2018

Abstract: The role of coagulation in acute lung injury (ALI) remains unclear. As factor Xa-dependent protease-activated receptor 2 (PAR-2) is reported to be an important target in blood coagulation and other processes, an inhibitor of factor Xa, rivaroxaban, was tested *in vivo* in C57BL/6 mice with ALI induced by intratracheal injections of lipopolysaccharide (LPS) and *in vitro* in LPS-stimulated human umbilical vein endothelial cells. Plasma concentrations and coagulation indices were measured in mice fed normal chow or chow containing rivaroxaban (0.2 or 0.4 mg/g) for 10 days. The rivaroxaban-treated mice had significantly reduced neutrophil sequestration with preservation of the lung tissue architecture compared with that in the untreated controls. The levels of tumor necrosis factor alpha, interleukin 1 beta, and interleukin 6, as well as total protein and Evans blue concentrations, were all significantly reduced in bronchoalveolar lavage fluid from mice treated with rivaroxaban. Rivaroxaban treatment also ameliorated the LPS-induced PAR-2 increase and nuclear factor kappa B (NF-κB) activation. *In vitro*, cells treated with rivaroxaban had higher cell viability with an attenuation of LPS-induced increases in membrane permeability and proinflammatory cytokine levels, as well as reduced apoptosis. Furthermore, rivaroxaban inhibited the phosphorylation of TAK1 and p65. These data show that rivaroxaban attenuates ALI and inflammation by inhibiting the PAR-2/NF-κB signaling pathway.

Keywords: Acute lung injury, endothelial cells, factor Xa, NF-κb, rivaroxaban

Introduction

Acute lung injury (ALI) is a critical hypoxemic respiratory failure characterized by vascular leakage, alveolar capillary membrane damage, severe neutrophil infiltration, and pulmonary edema secondary to endothelial barrier dysfunction [1], and its underlying pathological changes include hemorrhage and microvascular thrombosis [2]. A major cause of mortality for ALI is bacterial sepsis, in which lipopolysaccharide (LPS) and the endotoxins of Gram-negative bacteria contribute to inflammation, cytoskeleton remodeling, and endothelial barrier dysfunction [3]. The pathogenesis of ALI involves inflammation and, in particular, a procoagulant antifibrinolytic environment in the alveoli and within systemic circulation [2, 4]. A previous study showed that tumor necrosis factor alpha (TNF-α), interleukin 1 beta (IL-1β), and interleukin 6 (IL-6) increase tissue factors and inhibit fibrinolysis, thereby activating an extrinsic pathway, and that factor Xa (FXa), alpha thrombin, and fibrin increased the synthesis of IL-6 and IL-8 [5]. This "cross-talk" amplification of the coagulation and inflammatory cascades contributes to ALI [6].

Although the primary function of the coagulation cascade is to promote hemostasis and limit blood loss in response to tissue injury, it also plays a pivotal role in influencing inflammatory and repair responses to tissue injury [7]. Interestingly, bronchoalveolar lavage fluid (BALF) from mice with ALI and pulmonary fibrosis have elevated levels of thrombin and FXa [8], a serine protease that links the extrinsic and intrinsic pathways in the coagulation cas-

cade. Recent evidence also indicates that FXa has nonhematologic functions, such as mediating inflammation, vascular remodeling, and tissue fibrosis [9, 10] and increasing the transcription of inflammatory molecules [11, 12], which enhance tissue inflammation and remodeling and are primarily mediated by protease-activated receptors (PARs) [12-14]. PARs are a small family of G protein-coupled receptors that also mediate the cellular effects of thrombin and other proteases, such as trypsin and metalloproteinase [15]. PAR-2 is predominantly expressed in endothelial cells (ECs) in the vessel wall and, when activated, facilitates their conversion to a proinflammatory phenotype and increases vascular permeability and the exposure/secretion of proteins and cytokines that promote platelet and leukocyte accumulation [16-18].

Proper lung functioning requires intact tight epithelial and endothelial barriers and normal ion and water transport, which prevents alveolar flooding [19]. ECs attach to vessel walls to regulate blood flow and the delivery of cells and proteins to tissues [20, 21]. The loss of EC barrier function is tightly linked to agonist-induced cytoskeletal reorganization, which disrupts cell-cell contacts and promotes the formation of paracellular gaps. A failure to restore EC function can lead to the destruction of the blood-air barrier, which directly results in the leakage of lung tissue protein, thus initiating ALI [22, 23]. EC dysfunction can also lead to pulmonary permeability edema, a fatal complication of ALI. Thus, therapies that preserve or restore this vascular barrier are urgently needed.

A previous report found that rivaroxaban, an approved oral anticoagulant that inhibits FXa and the prothrombinase complex, suppresses the expression of inflammatory mediators [12]. To test whether rivaroxaban inhibits inflammatory cytokine release in ECs and attenuates damage from ALI, we administered rivaroxaban to mice with LPS-mediated lung injury and to LPS-treated ECs *in vitro*. In addition, the mechanism by which rivaroxaban affects signal transduction in ECs was studied.

Materials and methods

Reagents

Human umbilical vein ECs (HUVECs) were purchased from IBCB (Shanghai, China). Dulbecco's modified Eagle's medium (DMEM) and fetal bovine serum (FBS) were from Gibco of Thermo Fisher Scientific (Shanghai, China). FXa was purchased from Hematologic Technologies, Inc. (Essex Junction, VT, USA). Bacterial LPS and Evans blue (EB) were purchased from Sigma-Aldrich (St. Louis, MO, USA). Rivaroxaban was purchased from Janssen Pharmaceuticals (Beerse, Belgium) and processed to 0.4 mg/g and 0.2 mg/g chow in the SLAC Laboratory Animal Center (Shanghai, China). Specific monoclonal antibodies against p38, phospho-p38, JNK, phospho-JNK, p65, phospho-p65, TAK1, phospho-TAK1, and GAPDH were obtained from Cell Signaling Technology (Beverly, MA, USA). The anti-PAR-2 antibody was obtained from Abcam (Cambridge, MA, USA), and the anti-myeloperoxidase (MPO) antibody was purchased from R&D Systems, Inc. (Minneapolis, MN, USA). Enzyme-linked immunosorbent assay (ELISA) kits for measuring mouse IL-1β, IL-6, and TNF-α, as well as human IL-1β, IL-6, and TNF-α immunoassay kits, were obtained from R&D Systems, Inc. Protein concentrations were determined using the bicinchoninic acid (BCA) protein assay kit (Beyotime Institute of Biotechnology, Jiangsu, China). All other chemicals were of reagent grade.

Mice, animal sacrifice, and preparation of plasma and tissue

Male C57BL/6 mice (6 to 7 weeks old; average weight, 20 g) from the SLAC Laboratory Animal Center were used in this study. Animals were kept in a controlled environment with regulated temperature and humidity on a 12/12-h light/dark cycle with *ad libitum* access to chow and drinking water. Mice were fed normal chow (PBS and N-LPS groups) or chow containing rivaroxaban at 0.2 mg/g or 0.4 mg/g (L-LPS or H-LPS group, respectively) [14]. Body weights were measured just before LPS administration. Mice were anesthetized with an intraperitoneal injection of sodium pentobarbital and received intratracheal injections of either 2.5 μl/g body weight of 2 mg/ml LPS saline solution or an equivalent volume of phosphate-buffered saline (PBS) (**Figure 1A**). After 48 h, the mice were anesthetized for plasma, BALF, or lung histological analyses. All data represent 6 mice per group. Blood was collected in the morning, drawn from the left ventricle into 3.4% sodium citrate (9:1 ratio). Platelet-poor plasma was prepared in < 2 h via two

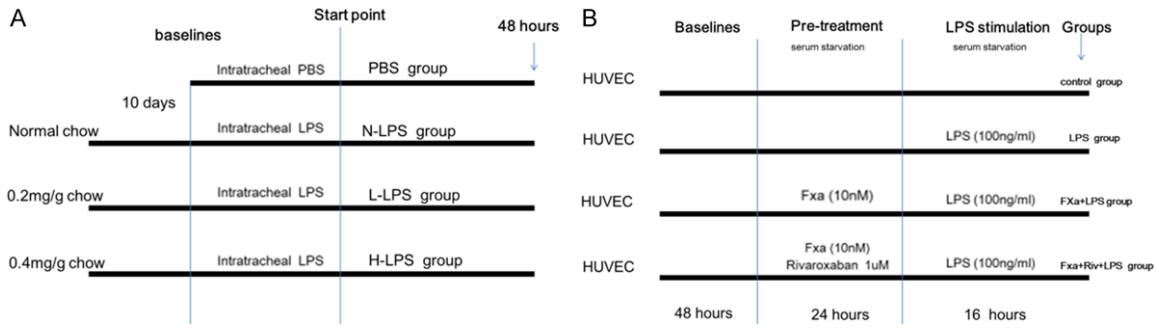

Figure 1. Schemes of the *in vitro* and *in vivo* models of ALI. A. Scheme of the LPS-induced ALI mouse model with or without rivaroxaban treatment. B. Scheme of the LPS-stimulated HUVEC model with or without rivaroxaban and FXa pretreatment.

sequential centrifugations to remove residual platelets: citrated blood was first centrifuged at 6,000 × *g* for 5 min at 4°C, and the supernatant was then centrifuged at 10,000 × *g* for 5 min at 4°C, aliquoted, and stored at -80°C until use [24]. BALF was obtained by instilling the left lung with 500 μl of precooled PBS and gently aspirating repeatedly three times. BALF was assessed for cell counts, protein content, EB amounts, and cytokine levels. Right lung lobes were removed to obtain formalin-fixed paraffin-embedded sections. Part of the lung tissue was snap-frozen in liquid nitrogen and stored at -80°C for qPCR and Western blot analyses. All experiments were approved by the University of Fudan Animal Care and Use Committee.

Assessment of coagulation in vivo

Tail bleeding times in mice were determined by amputating the tail 5 mm from the tip and immersing it in 0.9% isotonic saline at 37°C and recording the time to a complete arrest of bleeding. Plasma was collected in tubes containing one-tenth the volume of 3.4% sodium citrate to determine the activated partial thromboplastin time (APTT), prothrombin time (PT), and thrombin time (TT) with the appropriate reagents using a semiautomated coagulation analyzer.

Plasma concentrations of rivaroxaban

Plasma concentrations of rivaroxaban were determined by liquid chromatography-tandem mass spectrometry (LC-MS/MS) [25]. Linezolid was used as an internal standard, as it has structural similarities with rivaroxaban. Working solutions of 1,090 ng/ml, 545 ng/ml, 218 ng/ml, 109 ng/ml, 55 ng/ml, and 11 ng/ml rivaroxaban were obtained by mixing these stock solutions with linezolid. The concentration of dimethyl sulfoxide in plasma was 0.05%, which does not affect coagulation [26]. Sample preparation consisted of mixing methanol containing the internal standard and 100 μl of the plasma sample. The mixture was gently shaken and centrifuged. An aliquot (20 μl) of the final extract was injected into the LC-MS/MS system.

Lung wet-to-dry weight ratio

Wet-to-dry lung weight ratios were used as a measure of pulmonary edema. Mice were anesthetized, and the chest cavities were exposed. The lower lobe of the right lung of each mouse was removed and weighed on a piece of aluminum foil to determine the wet weight; the dry weight was obtained after the tissue was dried in an oven for 5 days at 60°C. The dry weights were monitored until two successive weights were similar, and the ratio was subsequently calculated as the net wet weight/net dry weight [27].

Lung permeability assessment

Lung permeability was assessed using the protein and EB dye concentrations in BALF samples and the EB dye extravasation method, as described previously [28]. Collected BALF was centrifuged at 500 × *g* for 10 min at 4°C, and the total protein content was measured by using a BCA protein assay kit according to the manufacturer's instructions. EB dye concentrations in BALF samples were calculated from a standard curve and are expressed as μg/ml. EB dye binds to circulating plasma proteins

and extravasates into the tissue at sites of increased vascular permeability [29]. For this method, EB dye at a dose of 50 mg/kg was injected into mice via the lateral tail vein 120 min before tissue collection. The left lung of each mouse was removed, and the dye was extracted in 2 ml formamide and 1 ml PBS solution at 60°C for 72 h. The optical density of the supernatant was measured at 620 nm. The results were normalized to the dry weight of the lung. The extravasated EB in lung tissue was expressed as μg of EB dye/g lung tissue.

Inflammatory cell counts in BALF

BALF samples were centrifuged at 500 × *g* for 10 min at 4°C. The cell-free supernatants were collected and frozen at -80°C for cytokine assays, and the pellets were lysed with red blood cell lysis buffer and resuspended in 100 μl PBS. Total cell counts were determined in cell suspensions using an animal blood counter. Then, 10 μl of the remaining cell suspension was used to prepare cytosmears by dripping onto glass slides. The smears were air-dried overnight prior to Giemsa-Wright staining to observe nucleated cells.

Morphological evaluation of lung sections

After opening the chest of each mouse, a portion of the right lung was removed, submerged and fixed in 10% buffered formalin, embedded in paraffin wax, and sectioned at 4 μm. Sections were stained with hematoxylin and eosin to semiquantitatively assess the severity of lung injury according to previously described methods with slight modifications. All histologic examinations were carried out in a double-blind manner using five images from each sample taken under × 100 magnification. The following pathological features were determined: i) focal alveolar membrane thickening; ii) capillary congestion; iii) intra-alveolar hemorrhage, iv) interstitial neutrophil infiltration, and v) intra-alveolar neutrophil infiltration. Each feature was scored from 0 to 3 on the basis of its absence (0) or presence to a mild (1), moderate (2), or severe (3) degree, and a cumulative total histology score was determined. The scores for each parameter from five images were averaged to obtain the mean for each sample.

Radiological analysis

To evaluate ALI, micro-computed tomography (micro-CT) high-spatial-resolution images were obtained of the entire thorax after 48 h of LPS administration. The mice were anesthetized and placed in the micro-CT chamber in the supine position. CT images were collected on a volumetric Siemens Inveon micro-CT scanner (Siemens, Germany) at 70 kVp and 500 μA. Images were acquired at 1,300 ms/frame, and 360° views and were reconstructed using the Feldkamp algorithm. The reconstructed images were 2,048 × 2,048 pixels, and the effective pixel size was 39.99 μm. The final reconstructed data were converted to the Digital Imaging and Communications in Medicine (DICOM) format by software (Lucion; MeviSYS, Seoul, South Korea).

Immunohistochemistry

Mouse lungs were embedded in paraffin, and 4-μm serial sections (300 μm apart) were obtained. For immunohistochemistry, paraffin sections were dewaxed, hydrated through a descending ethanol series, washed in 0.05 M Tris-HCl buffer (pH 7.6), placed in boiling citrate buffer (pH 5.8) for 10 min, and then allowed to cool at room temperature (RT) for 20 min. They were rinsed 3 × in Tris-buffered saline (pH 7.8) for 4 min each. Slides were placed in 50 ml of 0.5% trypsin solution, incubated in a water bath at 37°C for 15 min, and then rinsed 2 × in Tris-HCl buffer (pH 7.8) for 4 min each. The slides were then washed 2 × in PBS (pH 7.6) for 4 min each and blocked in 10% lamb serum for 30 min at RT before incubating with primary antibody overnight at 4°C. After three washes with PBS for 15 min, secondary antibodies were applied for 20 min at 37°C.

Cell culture and LPS treatment

HUVECs were maintained in DMEM supplemented with 1% penicillin/streptomycin and 10% FBS in an atmosphere of 5% CO_2 at 37°C and routinely passaged every 3 days. For analysis of the effect of rivaroxaban on proinflammatory activation, HUVECs were spread onto 100-mm or 60-mm tissue culture plates, grown to approximately 80% confluence, and treated with FXa (100 nM) with/without rivaroxaban (1,000 nM) for 24 h in serum-starved

and heparin-free conditioned medium. Then, some of the HUVEC monolayers were exposed to LPS (100 ng/ml) for 16 h. HUVECs were randomly divided into four groups as follows (**Figure 1B**): control group, cells were cultured in DMEM without serum, FXa, rivaroxaban, or LPS; LPS group, cells were cultured with LPS (100 ng/ml) for 16 h; FXa + LPS group, cells were cultured in serum-starved DMEM with FXa for 24 h before LPS was added; FXa + Riv + LPS group, cells were cultured in serum-starved DMEM with FXa and rivaroxaban for 24 h before LPS was added. After a 16-h treatment period, the cells and medium were collected for further experiments.

CCK-8 assay

Cells were separately seeded into four 96-well plates at a density of 1×10^4 cells with 100 µl medium in each well and incubated for 24 h in an atmosphere of 5% CO_2 at 37°C. To measure cell proliferation, 10 µl of the CCK-8 assay solution was added to each well, and the optical density at 450 nm was measured with a microplate reader after 2 h of incubation.

Wound healing assay

A wound healing assay was carried out to measure the motility of vascular ECs after treatment with rivaroxaban [30]. Briefly, 1×10^5 cells were seeded on 12-well plates and cultured for 48 h until full confluence was reached. After FXa and rivaroxaban pretreatment, the wells were then washed with PBS to remove nonadherent cells, and the cells in the middle of each well were scraped linearly with a 10-µl sterilized plastic pipette tip and induced with 100 ng/ml LPS for 16 h. The horizontal distance between the sides of the wound was photographed and measured with a digital microscope; data from three wells were averaged and experiments were performed in triplicates.

Annexin V-fluorescein isothiocyanate/propidium iodide (PI) staining for apoptosis determination

Apoptosis of HUVECs was assessed by flow cytometry. Briefly, trypsinized cells were washed with precooled PBS and incubated in the dark for 20 min at 4°C in 100 µl binding buffer containing 5 µl of Annexin V-fluorescein isothiocyanate. Next, the cells were stained with 3 µl of PI for 10 min. Fluorescence was determined by flow cytometry using CellQuest 5.1 software (BD Biosciences), and the data were analyzed with FlowJo software (Tree Star Inc., Ashland, OR, USA). The results were converted into percentages according to fluorescence intensity of the medium.

Endothelial permeability assay in vitro

Endothelial monolayer permeability assays were performed by measuring the flux of albumin-bound EB across functional HUVEC monolayers grown on Transwell polycarbonate membranes, as described previously [31, 32]. Briefly, a cell suspension (2×10^5 cells) was added to the upper chambers of the Transwell apparatus and cultured with 10% FBS DMEM overnight. After changing to serum-free medium, the HUVECs were exposed to FXa with or without rivaroxaban for 24 h followed by LPS (final concentration, 100 ng/ml) for 16 h. Next, 100 µl medium containing EB-conjugated bovine serum albumin (final concentration 0.67 mg/ml) was added to the Transwell inserts, while 600 µl medium containing 4% bovine serum albumin was added to the lower chamber. After incubation at 37°C for 1 h, the absorbance at 620 nm of 100 µl of medium from the lower chamber was measured.

Measurement of cytokines in HUVEC medium and BALF

HUVECs were grown to 80-90% confluence before treatment per the experimental conditions. To assess proinflammatory cytokine secretion, the supernatants were briefly centrifuged for 10 min at 500 × *g* to remove cell debris, the concentrations of TNF-a, IL-1β, and IL-6 were measured with commercially available human ELISA kits according to the manufacturer's instructions. In the animal studies, the analysis of TNF-a, IL-1β, and IL-6 in BALF supernatants was performed with mouse cytokine kits, according to the manufacturer's instructions.

Western blot analysis

Frozen lung tissues were homogenized and lysed in RIPA buffer. HUVECs were lysed using ice-cold RIPA buffer and protease inhibitor cocktail. Proteins were extracted by centrifugation at 14,000 × *g* for 5 min at 4°C, and the

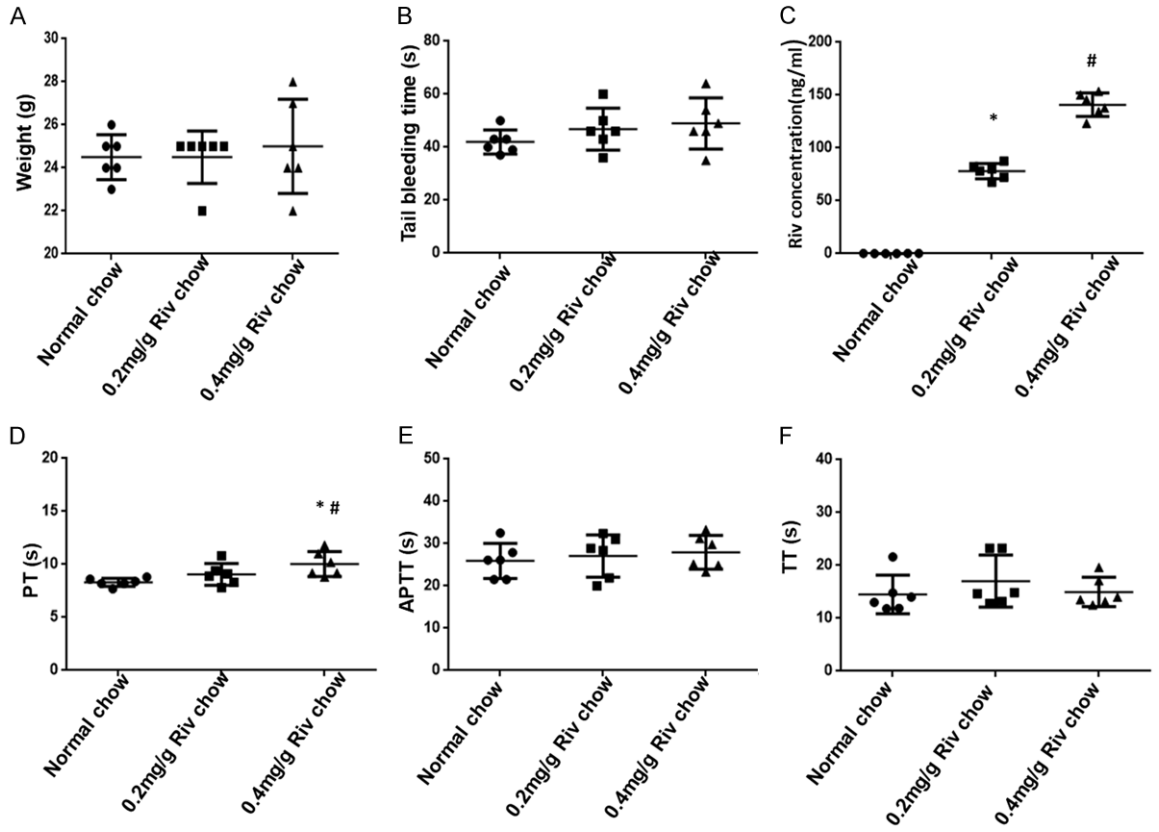

Figure 2. Baseline characteristics of the mice. (A) Average body weights of mice in groups fed normal chow or chow containing rivaroxaban (Riv) for 10 days. (B) Bleeding times were measured after a 5-mm section of the tail tip was cut. (C) Plasma concentrations of Riv. Prothrombin time (PT) (D), activated partial thromboplastin time (APTT) (E), and thrombin time (TT) (F). Data are the means ± SDs (n = 6). *P < 0.05 vs normal chow; #P < 0.05 vs 0.2 mg/g Riv chow.

protein concentrations were measured with a BCA protein assay kit. Samples of cell/tissue protein were mixed with loading buffer and separated by sodium dodecyl sulfate-polyacrylamide gel electrophoresis. The proteins were then transferred to polyvinylidene fluoride membranes by electrotransfer and blocked with 5% skim milk and 0.1% Tween 20 in PBS at RT for 2 h. The membranes were incubated with primary antibodies overnight at 4°C and then with horseradish peroxidase-conjugated secondary antibodies (1:1,000) at RT for 1.5 h. Images of protein bands were captured by a gel imaging system. The ratio of gray-scale values between the target protein band and the internal reference (β-actin or GAPDH) band was calculated as the relative protein expression using ImageJ.

Statistical analysis

All data were analyzed with GraphPad Prism 6 software (GraphPad Software Inc., La Jolla, CA, USA). The distance of cell migration and Western blot band intensities were measured using Image-Pro Plus 6 software (Media Cybernetics, Inc., Rockville, MD). One-way analyses of variance or the Student's t tests was used to compare data among or between groups, respectively. Pearson's X^2 or Fisher's exact tests were used to compare the percentages of apoptotic cells, the ratios of protein band intensities, and lung injury scores. For all tests, P values of < 0.05 were considered statistically significant.

Results

Baseline characteristics of mice with ALI

There were no notable differences among mice fed normal chow or those fed chow containing rivaroxaban with regard to body weight (**Figure 2A**) or average tail bleeding time (P = 0.30) (**Figure 2B**). As expected, the plasma concentration of rivaroxaban was significantly higher in

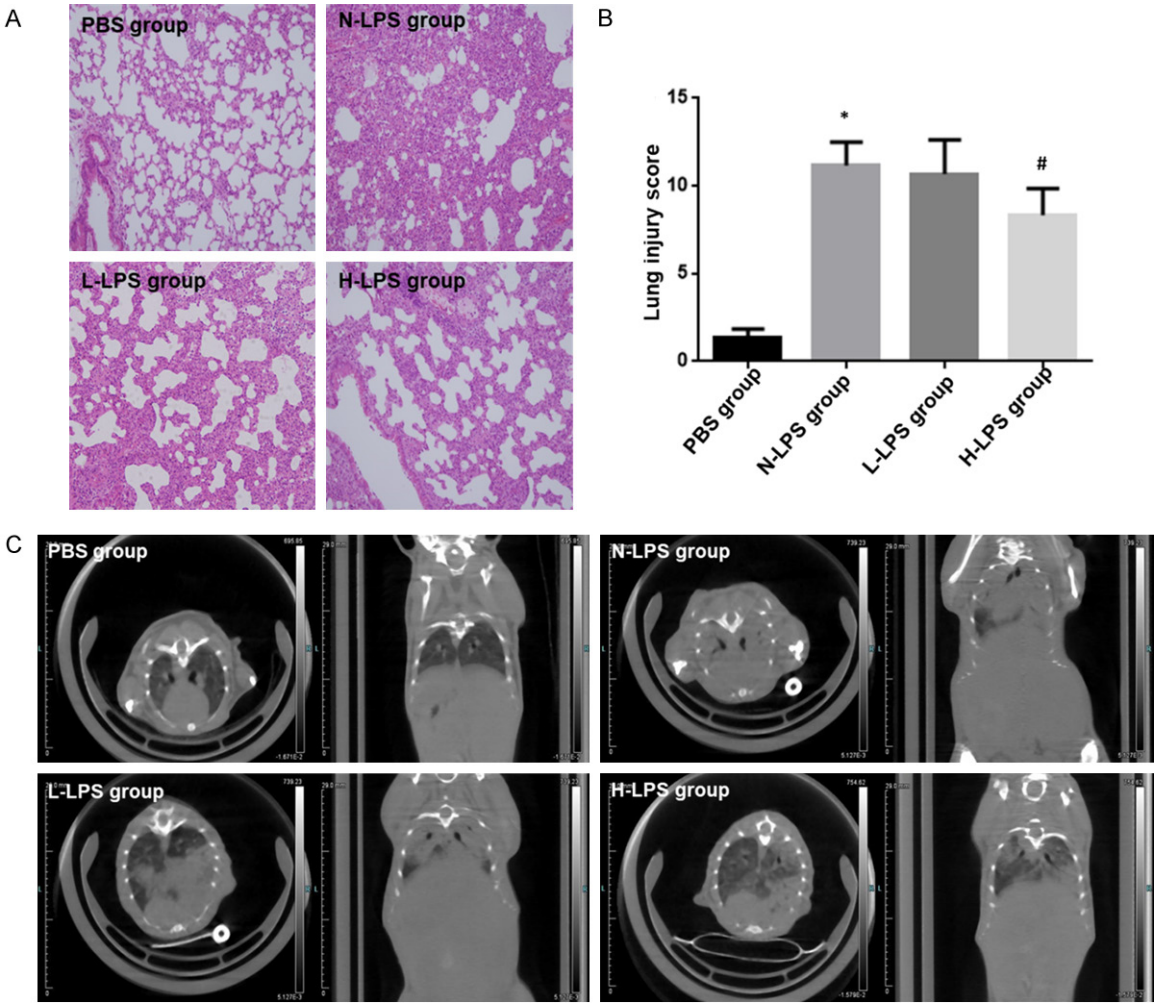

Figure 3. Effects of rivaroxaban on LPS-induced ALI in mice. A. Representative photomicrographs of mouse lungs (× 100 magnification). B. Mean semiquantitative distribution of total histology scores of lung injury in mice. Data are the means ± SDs (n = 6). *P < 0.05 vs PBS group; #P < 0.05 vs N-LPS group. C. Micro-computed tomography images of transverse sections showing lung injury severity in each treatment group.

mice fed chow containing 0.2 or 0.4 mg of rivaroxaban/g than in normal chow-fed controls (**Figure 2C**). Because mice are nocturnal, all measurements were performed in the morning to minimize the variability in the plasma drug levels due to differences in chow consumption. Although there was no difference among the groups with regard to TT and APTT values (P > 0.05), PT was significantly longer in mice fed chow containing 0.4 mg/g rivaroxaban (P < 0.01) (**Figure 2D-F**).

Rivaroxaban attenuates LPS-induced ALI in mice

To assess the effects of rivaroxaban on lung pathology, lung tissues from mice 48 h after a challenge with LPS were stained with hematoxylin and eosin (**Figure 3A**). According to the total histology scores, high-dose rivaroxaban reduced LPS-induced injury in the lungs compared with that in mice fed the normal diet, though the damage remained greater than that in sham-operated animals; however, low-dose rivaroxaban did not significantly alleviate injury (**Figure 3B**). Lung injury was also assessed by micro-CT, which revealed bilateral patchy infiltrates in LPS-treated mice (**Figure 3C**), in contrast to the normal radiological appearance of the lungs of mice in the control group. Infiltrates and injury were alleviated in the lungs of the rivaroxaban-treated mice.

Effects of rivaroxaban on cell viability, apoptosis, and migration of LPS-treated HUVECs

The effect of rivaroxaban on the viability of LPS-treated HUVECs was assessed with CCK8 cell

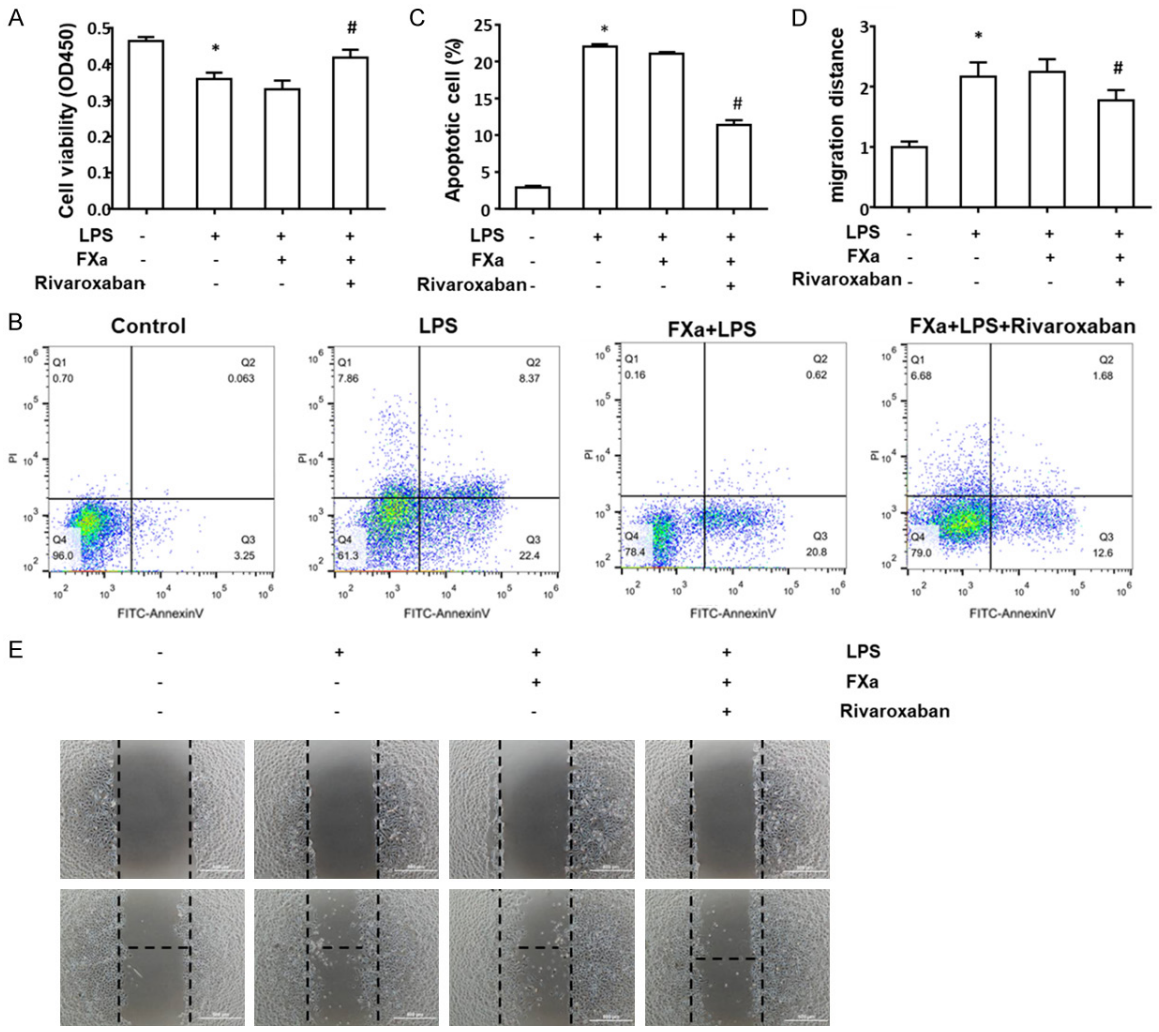

Figure 4. Effects of rivaroxaban on HUVEC viability, apoptosis, and migration. A. Viability was measured with a CCK-8 kit. B. Flow cytometry shows survival, necrosis, and apoptosis of cells stained with Annexin V and PI. Q1, necrotic cells; Q2, late apoptotic cells; B3, early apoptosis; Q4, viable cells. C. Percentages of apoptotic cells. D and E. Measurement of relative migration distance in wound healing assay. Data are the means ± SDs (n = 3). *P < 0.05 vs untreated controls; #P < 0.05 vs LPS-treated group.

viability kits. As shown in **Figure 4A**, cell viability was significantly decreased by exposure to LPS, and viability further decreased with FXa treatment, compared with that of the untreated control group. However, these decreases were attenuated with rivaroxaban, suggesting that the drug protects HUVECs against LPS-induced injury *in vitro*. As apoptosis also contributes to ALI/acute respiratory distress syndrome (ARDS) pathogenesis, flow cytometry was performed with Annexin V-PI double-stained HUVECs (**Figure 4B**). As shown in **Figure 4C**, LPS exposure significantly increased the percentage of apoptotic cells compared with that in the untreated control group, and this effect was significantly attenuated in cells pretreated with rivaroxaban. The highest percentage of apoptotic cells was observed in HUVECs treated with LPS, which was not significantly different from that of HUVECs treated with LPS and FXa. Next, the effect of rivaroxaban on LPS-induced HUVEC migration was assessed. As shown in **Figure 4D** and **4E**, stimulation of HUVECs with 100 ng/ml LPS for 16 h significantly spurred cell migration (2.17-fold vs control, P < 0.01). The migration of cells pretreated with FXa and rivaroxaban was decreased compared to that of cells treated with LPS alone (1.78-fold of

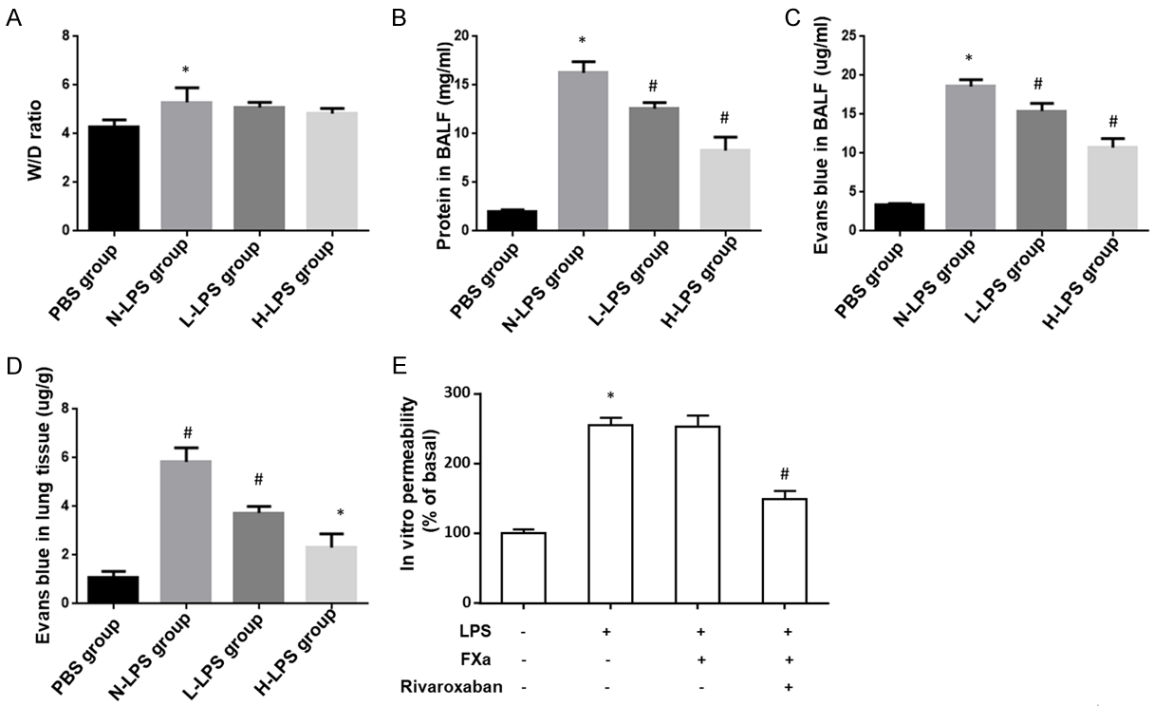

Figure 5. Effect of rivaroxaban on LPS-induced vascular endothelial permeability *in vivo* and *in vitro*. (A) Wet-to-dry lung weight (W/D) ratios. (B) Protein content in BALF samples estimated with a bicinchoninic acid protein assay kit. Lung vascular permeability was assessed by accumulation of Evans blue dye (injected 2 h before termination of the experiment) in BALF samples (C) and lung tissue (D). Data are the means ± SDs (n = 6). $^{*}P < 0.05$ vs PBS group; $^{\#}P < 0.05$ vs N-LPS group. (E) HUVEC monolayer permeability. Data are the means ± SDs (n = 3). $^{*}P < 0.05$ vs untreated controls; $^{\#}P < 0.05$ vs LPS–treated group.

the untreated group, $P < 0.05$). These results demonstrate that rivaroxaban significantly retarded HUVEC migration.

Rivaroxaban decreases LPS-induced vascular endothelial barrier permeability in vivo and in vitro

The wet-to-dry ratio of lung tissue weight was 4.3 ± 0.11 in mice in the PBS group and increased to 5.29 ± 0.25 in mice in the LPS group fed normal standard chow (N-LPS), which indicates there was fluid accumulation in the lungs (**Figure 5A**). However, the ratios did not differ between the LPS-treated animals fed normal chow and those fed rivaroxaban-containing chow. The albumin concentration in BALF represents the level of the effused albumin, and it was much higher in the LPS groups than in the PBS-treated group ($P < 0.05$). However, treatment with rivaroxaban (0.2 mg/g chow or 0.4 mg/g chow) substantially decreased the concentration of albumin in BALF (**Figure 5B**). To further assess EC barrier dysfunction, EB dye was injected via the caudal veins of mice 48 h after their LPS challenge, and EB extravasation in the BALF and lung tissue was determined 2 h later (**Figure 5C** and **5D**). Extravasation of EB was significantly higher in the LPS groups than in the PBS group ($P < 0.05$) but was significantly decreased in LPS-treated mice fed rivaroxaban-containing chow ($P < 0.05$ vs N-LPS group). Similarly, LPS induced the transendothelial transport of albumin-bound EB across an EC monolayer *in vitro*, whereas cells pretreated with rivaroxaban showed decreased EB transport (**Figure 5E**). Altogether, these observations strongly indicate that rivaroxaban protects ECs *in vitro* and may be protective against ALI *in vivo*.

Rivaroxaban suppresses inflammatory responses to LPS-induced ALI in vivo and in vitro

LPS elicits a robust inflammatory response and produces various effects linked to ALI. To determine whether the rivaroxaban-mediated protection against barrier dysfunction occurs due to the inhibition of inflammatory mediators affecting barrier integrity, we assessed the pro-

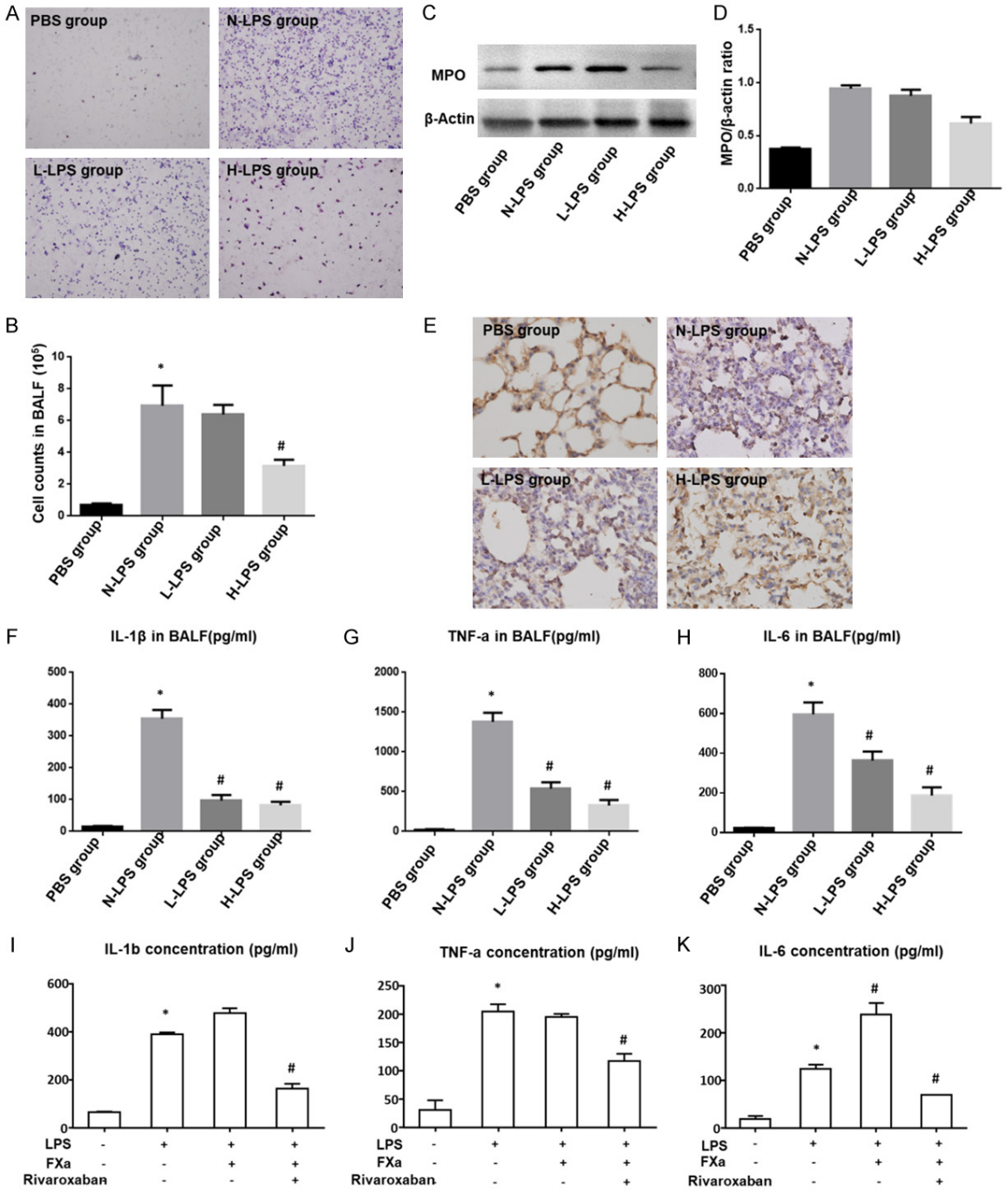

Figure 6. Effects of rivaroxaban on LPS-induced inflammatory responses *in vivo* and *in vitro*. (A) Representative images of Giemsa-stained cells from the BALF samples (× 100 magnification). (B) Quantitation of numbers of cells in the BALF samples. (C and D) Levels of MPO in lung tissue suggestive of neutrophil activation as shown by Western blot analysis. (E) Representative images of immunohistochemical staining for MPO (× 400 magnification). Concentrations of IL-1b (F), TNF-α (G), and IL-6 (H) in BALF samples. Data are the means ± SDs (n = 6). $^{*}P < 0.05$ vs PBS group; $^{\#}P < 0.05$ vs N-LPS group. Concentrations of IL-1b (I), TNF-α (J), and IL-6 (K) in medium from HUVECs. Data are the means ± SDs (n = 3). $^{*}P < 0.05$ vs untreated controls; $^{\#}P < 0.05$ vs LPS-treated group.

duction of inflammatory cytokines and inflammatory cell infiltration. The numbers of inflammatory cells in BALF samples increased dramatically (~8-fold) in response to LPS stimulation (**Figure 6A**). However, the total number of BALF cells significantly decreased by

55% in the animals fed chow containing 0.4 mg/g rivaroxaban (H-LPS group) compared to that of animals fed normal chow (N-LPS group); no significant decrease was observed in mice fed chow containing 0.2 mg/g rivaroxaban (L-LPS group) (**Figure 6B**). Neutrophil infiltration was also monitored by measuring MPO levels in lung tissue samples. LPS significantly increased MPO levels in tissue homogenates, indicative of neutrophil activation (**Figure 6C** and **6D**). Immunohistochemical staining revealed very low expression of MPO in lung tissues of mice from the PBS group, whereas staining dramatically increased in those treated with LPS (**Figure 6E**). Of note, the staining intensity substantially decreased in mice fed chow with high-dose rivaroxaban. Next, we performed ELISAs to measure the levels of inflammatory cytokines. In BALF samples from control mice, the levels of IL-1β, TNF-α, and IL-6 were very low. LPS treatment dramatically and significantly increased the levels of these three cytokines ($P < 0.01$), which were significantly attenuated by rivaroxaban treatment ($P < 0.05$) (**Figure 6F-H**). The effects of LPS and rivaroxaban on cytokine secretion were confirmed *in vitro*. The pretreatment of HUVECs with 1 μM rivaroxaban and 10 nM FXa suppressed the LPS-induced release of IL-1b, TNF-a, and IL-6 into the medium ($P < 0.01$) (**Figure 6I-K**). The results demonstrate that rivaroxaban inhibited the LPS-promoted inflammatory response *in vitro* and *in vivo*.

Rivaroxaban suppresses activation of the NF-κB pathway by PAR-2 following ALI in vivo and in vitro

To identify possible mechanisms underlying the protective effect of rivaroxaban on ALI, we examined the expression of PAR-2 in lung tissues. Immunohistochemical and Western blot analyses of lung tissues showed significantly increased expression of PAR-2 in LPS-treated mice, which was significantly decreased by treatment with rivaroxaban (**Figure 7A-C**). Together with the above results, the findings suggest that PAR-2 and its ligand FXa play a role in ALI pathogenesis. As coagulation factor VIIa/FXa-PAR-2 signaling activates NF-κB and MAPKs, which are major mediators of inflammation [9, 18, 33], we next examined whether the activation of these signaling pathways was involved. We found that LPS stimulation strongly induced the phosphorylation of the p65 NF-κB subunit in mouse lung tissue (**Figure 7D**). To explore this activation in more detail, we measured the phosphorylation of various signaling components in HUVECs stimulated with LPS *in vitro*. The pretreatment of HUVECs with FXa and its selective inhibitor rivaroxaban did not significantly suppress the LPS-induced phosphorylation of the MAPK proteins JNK and p38 (**Figure 7E-G**) but did significantly decrease the LPS-induced phosphorylation of TAK1 and p65 (**Figure 7E**, **7H**, and **7I**). These results suggest that rivaroxaban activates the TAK1 and p65 NF-κB signaling pathways via PAR-2 in LPS-induced ALI.

Discussion

Progressive ARDS is closely linked with inflammation and coagulation, which can be triggered by various coagulation proteases, such as FXa and thrombin [34]. Further elucidation of the subtle cross-talk between these processes may provide opportunities for unique therapeutic interventions in patients with ALI. In the present research, a direct inhibitor of FXa produced beneficial effects in a mouse model of ALI/ARDS, generated via intratracheal administration of LPS, and in HUVECs. Although LPS did not alter coagulation in mice, as assessed by APTT, TT, and PT (a measure of FII, FV, FX, and FVII activities), which is similar to previous results [7.5], the inhibition of FXa with rivaroxaban (0.4 mg/g chow) prolonged PT. Moreover, this dose of rivaroxaban (or 1 μM *in vitro*) ameliorated ALI and EC injury and dysfunction with concomitant reductions in inflammatory mediators. These effects were associated with decreased PAR-2 expression and activation of the NF-κB signaling pathway (**Figure 8**). Thus, rivaroxaban has anticoagulant effects and inhibits inflammatory responses in LPS-induced ALI.

Rivaroxaban, an orally administered FXa inhibitor, has been undergoing extensive clinical evaluations for the prevention and treatment of thromboembolic disorders. The high dose of rivaroxaban used in mice in the present study resulted in plasma levels of 141 ng/ml. In this study, this dose reduced not only the levels of inflammatory cytokines in BALF but also ALI progression, suggesting that rivaroxaban may prevent the development of lung injury via the inhibition of inflammatory activation.

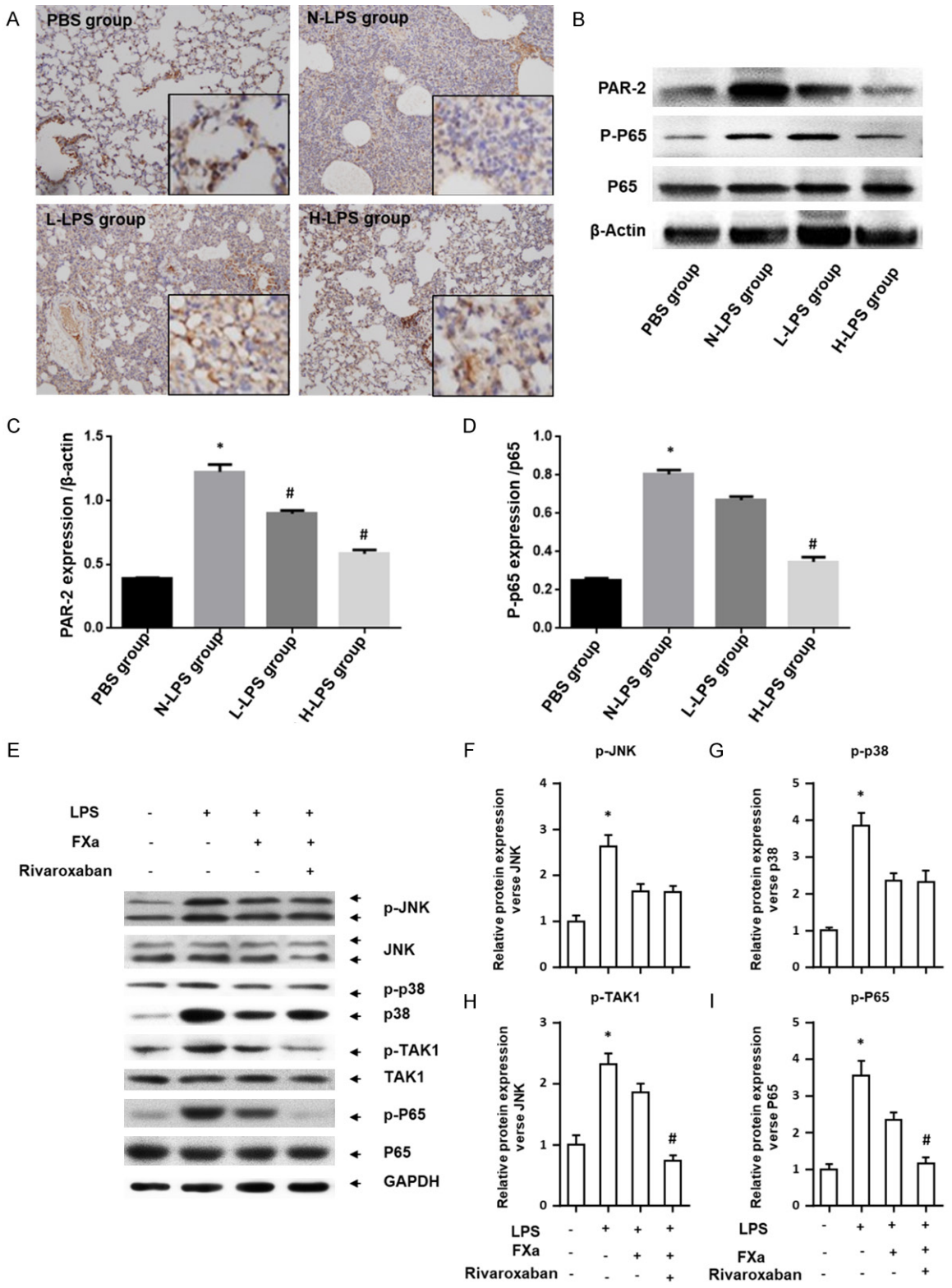

Figure 7. Effect of rivaroxaban on LPS-induced PAR-2 expression and signaling pathway activation *in vivo* and *in vitro*. (A) Immunohistochemical staining of PAR-2 in lung tissue (× 100 and × 400 [insets] magnification). (B) Western blot analysis of PAR-2, phospho-p65 (P-p65), and p65 NF-κB protein expression in lung tissue samples. Membrane probing with β-actin was used for normalization. Quantification of PAR-2 (C) and P-p65 (D) expression by ImageJ software. Data are the means ± SEMs (n = 6). *P < 0.05 vs PBS group; #P < 0.05 vs N–LPS group. (E) Representative Western blots for MAPK and NF-κB signaling in HUVECs. Quantification of P-JNK (F), P-p38 (G), P-TAK1 (H), and P-p65 (I) expression. Data are the means ± SEMs (n = 3). *P < 0.05 vs untreated controls; #P < 0.05 vs LPS–treated group.

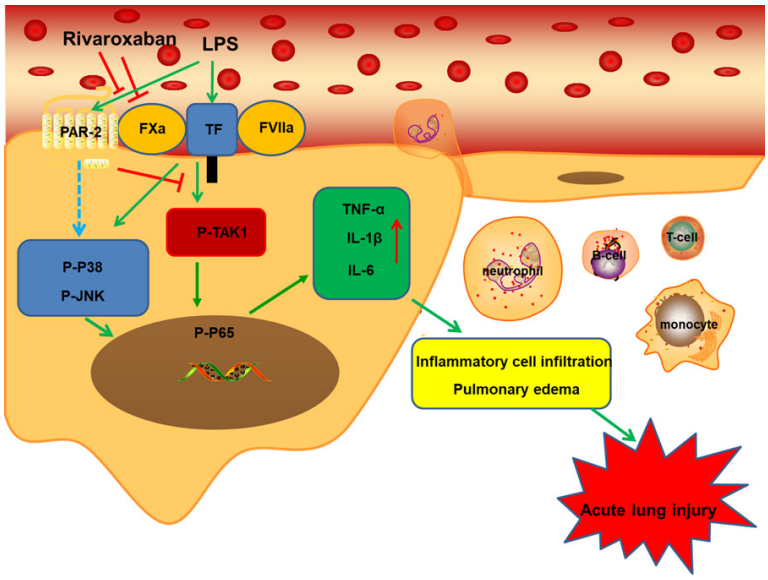

Figure 8. Schematic showing how inhibition of FXa attenuates ALI progression via modulation of the PAR-2/NF-κB signaling pathway.

Vascular EC injury and hyperpermeability play important roles in the development of LPS-induced ALI. These changes promote the release of cytokines and inflammatory responses, thereby exacerbating ARDS [35]. At the same time, the inflammatory cytokines promote leukocyte adhesion and coagulation activation and increase vascular permeability. Thus, the maintenance of endothelial barrier integrity is essential for vascular and tissue homeostasis [36]. In the present study, we found that LPS increased lung vascular endothelial permeability by altering the paracellular and transcellular barriers. Moreover, rivaroxaban reduced the albumin-bound EB content in the lower chamber of the Transwell assay, thereby retaining the integrity of the EC monolayer. Rivaroxaban also inhibited EC apoptosis, which plays an important role in various inflammatory diseases, and decreased the release of inflammatory cytokines. These results suggest that controlling inflammation at the level of ECs may efficiently retard or reverse the pathogenetic process in ALI. Therefore, understanding the differences among the signaling pathways of inflammatory factors is indispensable.

PAR-2 is activated by the tissue factor-coagulation factor VIIa complex and coagulation FXa and has crucial roles in inflammation and the regulation of vascular function. ECs highly express PAR-2 in response to inflammation, and PAR-2 stimulates cytokine release in HUVECs [18, 37, 38]. We demonstrated that LPS activates PAR-2 and promotes the production of cytokines in mice with ALI, which were suppressed by the inhibition of FXa with rivaroxaban. Previous studies have also demonstrated that coagulation factor VIIa/FXa-PAR-2 signaling activates NF-κB and MAPK, which are important regulators of cytokine production and are associated with the pathogenesis of inflammatory processes [9, 11, 38, 39]. Our results showed that these were activated by LPS and that pharmacologic pretreatment with rivaroxaban significantly attenuated NF-κB activation. Thus, the protection against LPS-induced lung injury both *in vivo* and *in vitro* may involve the inhibition of PAR-2 activity and NF-κB signaling, particularly via p65 phosphorylation. Altogether, these data suggest that rivaroxaban may be a new therapeutic option to relieve ALI via the suppression of PAR-2-NF-κB signaling and inflammation.

In conclusion, the present study demonstrates that in mouse lung tissue, FXa is an important coagulant factor and a mediator of inflammatory signaling via the activation of PAR-2 and NF-κB. LPS in lung tissue induces ALI by generating an inflammatory prothrombotic state. Importantly, LPS-induced inflammatory signaling and vascular EC activation can be substantially attenuated by an FXa antagonist and anticoagulant, rivaroxaban. Thus, rivaroxaban represents a novel therapeutic strategy to prevent and/or reduce the progression of ALI.

Acknowledgements

This study was supported by the Natural Science Foundation of China (81490533, 81400018, 81570028, 81500026, 81770039), the State Key Basic Research Program (973) project (2015CB553404), the Shanghai Science and Technology Committee (18140903400, 15DZ1930600, 15DZ1941103), and the Shanghai Three-Year Plan of the Key

Subjects Construction in Public Health-Infectious Diseases and Pathogenic Microorganism (15GWZK0102).

Disclosure of conflict of interest

None.

Address correspondence to: Dr. Xiaofeng Chen, Department of Cardiothoracic Surgery, Huashan Hospital, Fudan University, 12 Wulumuqi Middle Street, Shanghai 200040, China. Tel: 086-021-52887075; E-mail: hs_chenxiaofeng@yeah.net; Dr. Jie Hu, Department of Pulmonary Medicine, Zhongshan Hospital, Fudan University, 108 Fenglin Road, Xuhui District, Shanghai 200040, China. Tel: 086-021-64041990; E-mail: huashan_heart@sina.cn

References

[1] Aggarwal S, Gross CM, Kumar S, Dimitropoulou C, Sharma S, Gorshkov BA, Sridhar S, Lu Q, Bogatcheva NV, Jezierska-Drutel AJ, Lucas R, Verin AD, Catravas JD, Black SM. Dimethylarginine dimethylaminohydrolase II overexpression attenuates LPS-mediated lung leak in acute lung injury. Am J Respir Cell Mol Biol 2014; 50: 614-625.

[2] Glas GJ, Van Der Sluijs KF, Schultz MJ, Hofstra JJ, Van Der Poll T, Levi M. Bronchoalveolar hemostasis in lung injury and acute respiratory distress syndrome. J Thromb Haemost 2013; 11: 17-25.

[3] Czikora L, Sridhar S, Gorshkov B, Alieva IB, Kasa A, Gonzales J, Potapenko O, Umapathy NS, Pillich H, Rick FG, Block NL, Verin AD, Chakraborty T, Matthay MA, Schally AV, Lucas R. Protective effect of growth hormone-releasing hormone agonist in bacterial toxin-induced pulmonary barrier dysfunction. Front Physiol 2014; 5: 259.

[4] Idell S, James KK, Levin EG, Schwartz BS, Manchanda N, Maunder RJ, Martin TR, McLarty J, Fair DS. Local abnormalities in coagulation and fibrinolytic pathways predispose to alveolar fibrin deposition in the adult respiratory distress syndrome. J Clin Invest 1989; 84: 695-705.

[5] Russell JA. Genetics of coagulation factors in acute lung injury. Crit Care Med 2003; 31: S243-S247.

[6] Anthoni C, Russell J, Wood KC, Stokes KY, Vowinkel T, Kirchhofer D, Granger DN. Tissue factor: a mediator of inflammatory cell recruitment, tissue injury, and thrombus formation in experimental colitis. J Exp Med 2007; 204: 1595-1601.

[7] Fouassier M, Souweine B, Sapin AF, Hashemzadeh A, Marques-Verdier A, Caillaud D. Increase in proinflammatory cytokines in peripheral blood without haemostatic changes after LPS inhalation. Thromb Res 2009; 124: 584-587.

[8] Scotton CJ, Krupiczojc MA, Königshoff M, Mercer PF, Lee YC, Kaminski N, Morser J, Post JM, Maher TM, Nicholson AG, Moffatt JD, Laurent GJ, Derian CK, Eickelberg O, Chambers RC. Increased local expression of coagulation factor X contributes to the fibrotic response in human and murine lung injury. J Clin Invest 2009; 119: 2550-2563.

[9] Borensztajn K, Peppelenbosch MP and Spek CA. Factor Xa: at the crossroads between coagulation and signaling in physiology and disease. Trends Mol Med 2008; 14: 429-440.

[10] Schwientek P, Ellinghaus P, Steppan S, D'Urso D, Seewald M, Kassner A, Cebulla R, Schulte-Eistrup S, Morshuis M, Röfe D, El Banayosy A, Körfer R, Milting H. Global gene expression analysis in nonfailing and failing myocardium pre- and postpulsatile and nonpulsatile ventricular assist device support. Physiol Genomics 2010; 42: 397-405.

[11] Bukowska A, Zacharias I, Weinert S, Skopp K, Hartmann C, Huth C, Goette A. Coagulation factor Xa induces an inflammatory signaling by activation of protease-activated receptors in human atrial tissue. Eur J Pharmacol 2013; 718: 114-123.

[12] Hara T, Fukuda D, Tanaka K, Higashikuni Y, Hirata Y, Nishimoto S, Yagi S, Yamada H, Soeki T, Wakatsuki T, Shimabukuro M, Sata M. Rivaroxaban, a novel oral anticoagulant, attenuates atherosclerotic plaque progression and destabilization in ApoE-deficient mice. Atherosclerosis 2015; 242: 639-646.

[13] Esmon CT. Targeting factor Xa and thrombin: impact on coagulation and beyond. Thromb Haemost 2014; 111: 625-633.

[14] Sparkenbaugh EM, Chantrathammachart P, Mickelson J, van Ryn J, Hebbel RP, Monroe DM, Mackman N, Key NS, Pawlinski R. Differential contribution of FXa and thrombin to vascular inflammation in a mouse model of sickle cell disease. Blood 2014; 123: 1747-1756.

[15] Alberelli MA, De Candia E. Functional role of protease activated receptors in vascular biology. Vascul Pharmacol 2014; 62: 72-81.

[16] Su X, Matthay MA. Role of protease activated receptor 2 in experimental acute lung injury and lung fibrosis. Anat Rec (Hoboken) 2009; 292: 580-586.

[17] Osuga Y, Hirota Y, Yoshino O, Hirata T, Koga K, Taketani Y. Proteinase-activated receptors in the endometrium and endometriosis. Front Biosci (Schol Ed) 2012; 4: 1201-1212.

[18] Oe Y, Hayashi S, Fushima T, Sato E, Kisu K, Sato H, Ito S, Takahashi N. Coagulation factor Xa and protease-activated receptor 2 as novel

therapeutic targets for diabetic nephropathy. Arterioscler Thromb Vasc Biol 2016; 36: 1525-1533.
[19] Bhattacharya J, Matthay MA. Regulation and repair of the alveolar-capillary barrier in acute lung injury. Annu Rev Physiol 2013; 75: 593-615.
[20] Matthay MA, Zimmerman GA. Acute lung injury and the acute respiratory distress syndrome: four decades of inquiry into pathogenesis and rational management. Am J Respir Cell Mol Biol 2005; 33: 319-327.
[21] Orfanos SE, Mavrommati L, Korovesi L, Roussos C. Pulmonary endothelium in acute lung injury: from basic science to the critically ill. Intensive Care Med 2004; 30: 1702-1714.
[22] Rubenfeld GD, Caldwell E, Peabody E, Weaver J, Martin DP, Neff M, Stern EJ and Hudson LD. Incidence and outcome of acute lung injury. N Engl J Med 2005; 353: 1685-1693.
[23] Goldenberg NM, Steinberg BE, Slutsky AS and Lee WL. Broken barriers: a new take on sepsis pathogenesis. Sci Transl Med 2011; 3: 88ps25.
[24] Alame G, Mangin PH, Freund M, Riehl N, Magnenat S, Petitou M, Hechler B, Gachet C. EP217609, a neutralisable dual-action FIIa/FXa anticoagulant, with antithrombotic effects in arterial thrombosis. Thromb Haemost 2015; 113: 385-395.
[25] Rohde G. Determination of rivaroxaban--a novel, oral, direct Factor Xa inhibitor--in human plasma by high-performance liquid chromatography-tandem mass spectrometry. J Chromatogr B Analyt Technol Biomed Life Sci 2008; 872: 43-50.
[26] Camici GG, Steffel J, Akhmedov A, Schafer N, Baldinger J, Schulz U, Shojaati K, Matter CM, Yang Z, Lüscher TF, Tanner FC. Dimethyl sulfoxide inhibits tissue factor expression, thrombus formation, and vascular smooth muscle cell activation: a potential treatment strategy for drug-eluting stents. Circulation 2006; 114: 1512-1521.
[27] Becker PM, Kazi AA, Wadgaonkar R, Pearse DB, Kwiatkowski D, Garcia JG. Pulmonary vascular permeability and ischemic injury in gelsolin-deficient mice. Am J Respir Cell Mol Biol 2003; 28: 478-484.
[28] Duan Y, Learoyd J, Meliton AY, Leff AR, Zhu X. Inhibition of Pyk2 blocks lung inflammation and injury in a mouse model of acute lung injury. Respir Res 2012; 13: 4.
[29] Peng X, Hassoun PM, Sammani S, McVerry BJ, Burne MJ, Rabb H, Pearse D, Tuder RM, Garcia JG. Protective effects of sphingosine 1-phosphate in murine endotoxin-induced inflammatory lung injury. Am J Respir Crit Care Med 2004; 169: 1245-1251.
[30] Galley HF, Dhillon JK, Paterson RL, Webster NR. Effect of ciprofloxacin on the activation of the transcription factors nuclear factor kappaB, activator protein-1 and nuclear factor-interleukin-6, and interleukin-6 and interleukin-8 mRNA expression in a human endothelial cell line. Clin Sci (Lond) 2000; 99: 405-410.
[31] Lee W, Kim KM, Bae JS. Ameliorative effect of aspalathin and nothofagin from Rooibos (Aspalathus linearis) on HMGB1-induced septic responses in vitro and in vivo. Am J Chin Med 2015; 43: 991-1012.
[32] Shelton JL, Wang L, Cepinskas G, Sandig M, Inculet R, McCormack DG, Mehta S. Albumin leak across human pulmonary microvascular vs umbilical vein endothelial cells under septic conditions. Microvasc Res 2006; 71: 40-47.
[33] Krupiczojc MA, Scotton CJ, Chambers RC. Coagulation signalling following tissue injury: focus on the role of factor Xa. Int J Biochem Cell Biol 2008; 40: 1228-1237.
[34] Madoiwa S. Recent advances in disseminated intravascular coagulation: endothelial cells and fibrinolysis in sepsis-induced DIC. J Intensive Care 2015; 3: 8.
[35] Borissoff JI, Spronk HM, ten Cate H. The hemostatic system as a modulator of atherosclerosis. N Engl J Med 2011; 364: 1746-1760.
[36] Komarova YA, Kruse K, Mehta D, Malik AB. Protein interactions at endothelial junctions and signaling mechanisms regulating endothelial permeability. Circ Res 2017; 120: 179-206.
[37] Zhang R, Ge J. Proteinase-activated receptor-2 modulates ve-cadherin expression to affect human vascular endothelial barrier function. J Cell Biochem 2017; 118: 4587-4593.
[38] Banfi C, Brioschi M, Barbieri SS, Eligini S, Barcella S, Tremoli E, Colli S, Mussoni L. Mitochondrial reactive oxygen species: a common pathway for PAR1- and PAR2-mediated tissue factor induction in human endothelial cells. J Thromb Haemost 2009; 7: 206-216.
[39] Rothmeier AS, Ruf W. Protease-activated receptor 2 signaling in inflammation. Semin Immunopathol 2012; 34: 133-149.